

Dynamic Modeling of Multi-body Systems: A Numerical Study on Crank-slider Mechanism

Zanyu Jiang

The High School Affiliated to Renmin University of China, Beijing 100000, China.

Abstract

This paper aims to build a dynamical model on a crank-slider system under constant rotation and acquire numerical results with high accuracy and stability. The equations of motion are formulated for the system, while order reduction, the Baumgarte stabilization method, and Heun's method are integrated for our numerical solution strategy. A parameter sweep is conducted for optimal stabilization parameter choice that minimizes constraint violation. We thereby propose a closed-loop system that iteratively updates the system's generalized coordinates and external torque with feedback from current violation. Numerical error is shown to be suppressed well in the stability analysis. The resulting generalized coordinates and external torque exhibit smooth periodic oscillation that fits well with theoretical prediction, with peak external torque increasing with the required rotational speed.

Keywords

Multi-body dynamics; Crank-slider mechanism; Numerical simulation; Constraint stabilization

<https://oajrcap.damray.com/>

OPEN ACCESS

DOI: 10.26855/oajrcap.2025.12.001

Received: October 28, 2025

Accepted: November 25, 2025

Published: December 22, 2025

Copyright: ©2025 Zanyu Jiang. This is an open access article distributed under the terms of the Creative Commons Attribution License, which permits unrestricted use, distribution, and reproduction in any medium, provided the original author and source are credited.

1. Introduction

A multibody system (MBS) is composed of a group of rigid or deformable bodies connected by joints and acted upon by forces [1], which is widely applicable in fields of machines, vehicles, robotic manipulators, and space structures [2]. Dynamical responses of these systems often play a critical role in their durability and key performances. For example, it has been found that collisions in joints with clearances could lead to vibration and chaotic behavior in machines [3], and that excitations from wheel polygonization induce fatigue in the gearbox [4]. Therefore, establishing efficient dynamical models is crucial for predicting behavior and optimizing design in mechanical systems.

Extensive research efforts have been devoted to the development of multi-body dynamics. While dynamical equation forms the basis of simulation, classical approaches of the Newton-Euler method and Lagrange method perform unnecessary operations by calculating non-working constraint forces. Kane's equations [5] address this weakness by eliminating such forces, yielding higher computation efficiency. Analysis of the impact of imperfect joints is also a subfield that attracts many researchers. Early work of Dubowsky and Freudenstein established a model where surface compliance is linearized as a spring element, and a simple viscous coefficient models the damping [6]. To address the numerical difficulties associated with this approach, Khulief and Shabana derived an algebraic impulse-momentum balance equation that is able to describe jump discontinuities in velocities and contact

forces [7].

In terms of flexible multi-body systems, the floating frame of reference formulation by Shabana is a widely used method that constructs one reference frame to account for the body's motion, while a second one describes the deformation with respect to the first one [2]. The absolute nodal coordinate formulation is also proposed by Shabana, which defines finite elements by global coordinates and is widely applied in large deformation situations [8]. More recently, there has been a growing interest in applying machine learning in multi-body simulation for lower modeling difficulty, cost, and calculation amount. A 2021 study by Ye et al. proposed a deep learning model able to predict the dynamical behavior of a multi-body system with low frequency accurately and quickly [9]. In addition, Koutsoukakis et al. trained a CNN classifier to monitor gear transmission condition, achieving high prediction accuracy on experimental data [10].

From the literature, it can be seen that the dynamic modeling of multi-body systems attracts the attention of many researchers. Aiming at the same objective, this work is directed toward modeling a crank-slider system under constant rotation and investigating its dynamical responses via numerical methods. The rest of the paper is organized as follows. Section 2 offers a brief description of the investigated system, listing the generalized coordinates and system parameters. Section 3 includes the formulation of dynamical equations of the system and the method for computing external torque input. Section 4 presents the stability and integration method used. The simulation results are discussed in Section 5, and the last section summarizes the paper.

2. System Description

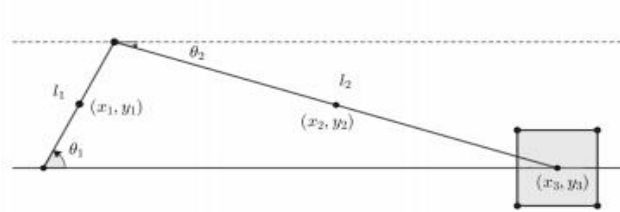


Figure 1. System schematic.

This paper investigates a slider-crank system consisting of a crank of length l_1 , a linkage of length l_2 , and a slider. Concentrated masses m_1 and m_2 are located at the midpoints of the crank and linkage, respectively, and the slider has a mass of m_3 . The slider is constrained to move in the horizontal direction, while an external torque is applied to the crank for constant rotation at angular velocity ω . The relevant parameters are listed in Table 1. Using Cartesian coordinates, we establish the generalized coordinates of the system as follows:

$$\mathbf{q} = [x_1, y_1, \theta_1, x_2, y_2, \theta_2, x_3] \text{ T} \quad (1)$$

Table 1. System Parameters

l_1	l_2	m_1	m_2	m_3
60 mm	180 mm	0.5 kg	1.2 kg	2.0 kg

where \mathbf{q} denotes the position vector. (x_1, y_1) and (x_2, y_2) each represent the position of the center of mass of the crank and the linkage, and x_3 is the x-coordinate of the slider. In addition, θ_1 corresponds to the angle of the crank from the horizontal, and θ_2 is the angle of the linkage.

3. Dynamic Analysis

3.1 Kinematic analysis

The position constraint of the system can be derived from the geometric relationship between the coordinates, as well as the driver constraint. Its general form is expressed as:

$$\Phi(\mathbf{q}, t) = 0 \quad (2)$$

where Φ denotes the constraint vector, \mathbf{q} denotes the generalized coordinate vector, and t denotes the time variable. In this modeled slider-crank system, the set of equations is derived as follows:

$$(\mathbf{q}, t) = \begin{bmatrix} x_1 - \frac{1}{2}l_1 \cos \theta_1 \\ y_1 - \frac{1}{2}l_1 \sin \theta_1 \\ \theta_1 - \omega t \\ x_2 - l_1 \cos \theta_1 - \frac{1}{2}l_2 \cos \theta_2 \\ y_2 - l_1 \sin \theta_1 - \frac{1}{2}l_2 \sin \theta_2 \\ l_1 \sin \theta_1 + l_2 \sin \theta_2 \\ x_3 - l_1 \cos \theta_1 - l_2 \cos \theta_2 \end{bmatrix} = 0 \quad (3)$$

The velocity and acceleration constraints of the system can be obtained by taking the time derivative of equation 3. We first derive the velocity constraint:

$$\boldsymbol{\varphi} \dot{\boldsymbol{\varphi}} = 0 \rightarrow \boldsymbol{\varphi}_q \dot{\mathbf{q}} = -\boldsymbol{\varphi}_t = \mathbf{v} \quad (4)$$

where $\boldsymbol{\varphi} \cdot$ denotes the time derivative of the constraint equations, $\boldsymbol{\varphi}_q$ is the partial derivative of the constraint equations $\boldsymbol{\varphi}$ with respect to the generalized coordinates \mathbf{q} , and $\boldsymbol{\varphi}_t$ represents the partial derivative of the constraint equations $\boldsymbol{\varphi}$ with respect to time.

The second-order time differentiation of the constraint equation yields:

$$\ddot{\boldsymbol{\varphi}} = (\boldsymbol{\varphi}_{qq})_q \dot{\mathbf{q}} + \boldsymbol{\varphi}_{q\ddot{q}} + 2\boldsymbol{\varphi}_{qt} \dot{\mathbf{q}} + \boldsymbol{\varphi}_{tt} = 0$$

which can be rewritten as

$$\boldsymbol{\Phi}_q \ddot{\mathbf{q}} = -(\boldsymbol{\Phi}_q \dot{\mathbf{q}})_q \dot{\mathbf{q}} - 2\boldsymbol{\Phi}_{qt} \dot{\mathbf{q}} - \boldsymbol{\Phi}_{tt} = \boldsymbol{\gamma} \quad (5)$$

The right-hand side of the acceleration equations $\boldsymbol{\gamma}$ is derived as the following vector in the investigated system:

$$\boldsymbol{\gamma} = \begin{bmatrix} -\frac{l_1}{2} \omega^2 \cos \theta_1 \\ -\frac{l_1}{2} \omega^2 \sin \theta_1 \\ 0 \\ -l_1 \omega^2 \cos \theta_1 - \frac{l_2}{2} \cos \theta_2 (\dot{\theta}_2)^2 \\ -l_1 \omega^2 \sin \theta_1 - \frac{l_2}{2} \sin \theta_2 (\dot{\theta}_2)^2 \\ l_1 \omega^2 \sin \theta_1 + l_2 \omega^2 \sin \theta_2 (\dot{\theta}_2)^2 \\ -l_1 \omega^2 \cos \theta_1 - l_2 \cos \theta_2 (\dot{\theta}_2)^2 \end{bmatrix}$$

The entire kinematic analysis follows the workflow shown in Figure 2. We start by constructing position constraints, then deriving the kinematic constraints at the velocity and acceleration levels. These forms system of linear equations that are solvable for $\dot{\mathbf{q}}$ and $\ddot{\mathbf{q}}$. Through integration, we update the generalized coordinates after one-time step Δt , and begin a new iteration. Repeating the above procedure yields a continuous numerical solution of the system's kinematics over a given time range of tend.

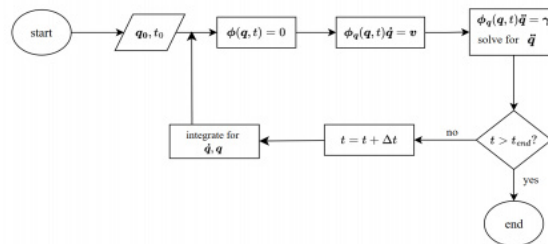


Figure 2. Workflow.

3.2 Formulation of equations of motion

The force constraint equation of a constrained system is written as: $\mathbf{M} \ddot{\mathbf{q}} = \mathbf{g} + \mathbf{g}_c$.

where \mathbf{g} is the general force vector, \mathbf{g}_c is the constraint force vector, and \mathbf{M} is the generalized mass matrix. In our system, \mathbf{M} and \mathbf{g} are expressed as

$$\mathbf{M} = \begin{bmatrix} m_1 & 0 & 0 & 0 & 0 & 0 & 0 \\ 0 & m_1 & 0 & 0 & 0 & 0 & 0 \\ 0 & 0 & J_1 & 0 & 0 & 0 & 0 \\ 0 & 0 & 0 & m_2 & 0 & 0 & 0 \\ 0 & 0 & 0 & 0 & m_2 & 0 & 0 \\ 0 & 0 & 0 & 0 & 0 & J_2 & 0 \\ 0 & 0 & 0 & 0 & 0 & 0 & m_3 \end{bmatrix} \mathbf{g} = \begin{bmatrix} 0 \\ -m_1 g \\ \tau \\ 0 \\ -m_2 g \\ 0 \\ 0 \end{bmatrix}$$

where J_1 J_2 is the rotational inertia of the crank and linkage, and τ is the external torque input into the system. By introducing the lagrangian multiplier and writing \mathbf{g}_c as $-\phi_q^T \lambda$, the force equilibrium equation can be written as

$$\mathbf{M} \ddot{\mathbf{q}} + \phi_q^T \lambda = \mathbf{g}$$

Together with the kinematic constraint equation 5, we now write the dynamic constraint matrix for our slider-crank system

$$\begin{bmatrix} \mathbf{M} & \phi_q^T \\ \phi_q & 0 \end{bmatrix} \begin{bmatrix} \ddot{\mathbf{q}} \\ \lambda \end{bmatrix} = \begin{bmatrix} \mathbf{g} \\ \gamma \end{bmatrix} \quad (6)$$

[11] where it constructs a linear system that is solvable for $\ddot{\mathbf{q}}$ and λ .

3.3 External Torque Computation

This subsection details the computation of the external torque τ required to maintain the constrained rotation of the crank. The calculation proceeds via a process of elimination and back-substitution.

Substituting the specific elements of into (6) yields a set of 14 linear equations.

The system is simplified by noting that the third generalized acceleration $\ddot{\theta}_3 = \ddot{\theta}_1 = 0$. Thus, the third column of the 14×14 matrix can be eliminated, as its contribution to the system is null. We further notice that row 9 and column 9 of the matrix are all composed of zero elements after this operation, so these are also removed. The system is thereby converted into 12 linear equations, where all elements λ are known. Once the reduced system is solved, the complete dynamics are known. Torque τ is then computed by back-substituting the solution into the third original equation:

$$\tau = [\mathbf{M} \quad \phi_q^T]_{(3)} \begin{bmatrix} \ddot{\mathbf{q}} \\ \lambda \end{bmatrix} \quad (7)$$

4. Numerical Solution Strategy

4.1 Order Reduction for Direct Integration

When acquiring the numerical solution of the system's generalized coordinates, direct integration of \mathbf{q} ... twice accumulates error significantly. We address this issue by adopting the method of reduced order.

By introducing a vector \mathbf{Q} consisting of generalized coordinates \mathbf{q} and its velocity $\dot{\mathbf{q}}$

$$\mathbf{Q} = \begin{bmatrix} \mathbf{q} \\ \dot{\mathbf{q}} \end{bmatrix}$$

The generalized acceleration $\ddot{\mathbf{q}}$ can be expressed as part of the time derivative of \mathbf{Q} :

$$\dot{\mathbf{Q}} = \begin{bmatrix} \dot{\mathbf{q}} \\ \ddot{\mathbf{q}} \end{bmatrix}$$

Then the original second-order differentiation system is transformed into a first-order form that only requires one integration from \mathbf{Q}^* to \mathbf{Q} . Common numerical methods for ODE are now applicable, and the system can be solved for $\ddot{\mathbf{q}}$ and λ continuously.

4.2 Constraint Stabilization via the Baumgarte Method

While the reduced-order system is now solvable, direct integration leads to accumulating constraint violation. The Baumgarte Stability method is introduced to address this issue, and its workflow is shown in Figure 3. The acceleration constraint is replaced with

$$\ddot{\phi} + 2\alpha\dot{\phi} + \beta^2\phi = 0$$

where a closed-loop system is constructed to damp the acceleration constraint with feedback from constraint violation at the velocity and position level. The stabilization parameters α and β are typically chosen as $\alpha = \beta = 1/\Delta t$ to produce critical damping, where Δt is the integration time step.

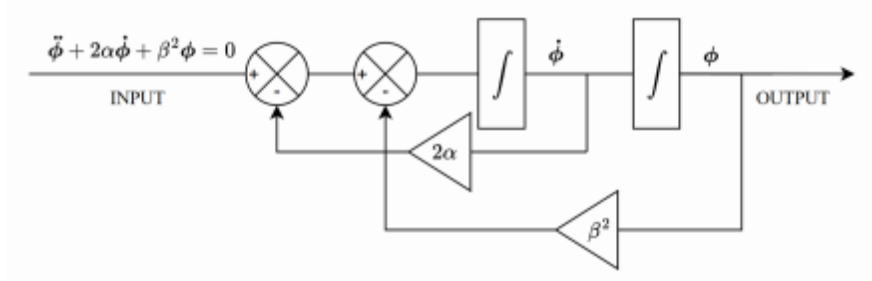


Figure 3. Workflow.

Consequently, the constraint matrix reforms into the following:

$$\begin{bmatrix} \mathbf{M} & \phi_q^T \\ \phi_q & \mathbf{0} \end{bmatrix} \begin{bmatrix} \ddot{\mathbf{q}} \\ \lambda \end{bmatrix} = \begin{bmatrix} \mathbf{g} \\ \gamma - 2\alpha\dot{\phi} - \beta^2\phi \end{bmatrix} \quad (8)$$

4.3 Numerical solution via Heun's method

The numerical solution of the generalized coordinates can now be acquired using Heun's integration method. We first acquire the generalized coordinates and velocity at the current state:

$$\frac{d\mathbf{Q}_i}{dt} = f(t_i, \mathbf{Q}_i)$$

Then compute the predicted time derivative of state vector $\left(\frac{d\mathbf{Q}_{i+1}}{dt}\right)^p$ at the next time step:

$$\left(\frac{d\mathbf{Q}_{i+1}}{dt}\right)^p = f\left(t_{i+1}, \mathbf{Q}_i + \Delta t \cdot \frac{d\mathbf{Q}_i}{dt}\right)$$

And calculate the corrected state vector

$$\mathbf{Q}_{i+1} = \mathbf{Q}_i + \frac{\Delta t}{2} \cdot \left[\frac{d\mathbf{Q}_i}{dt} + \left(\frac{d\mathbf{Q}_{i+1}}{dt}\right)^p\right] \quad (9)$$

5. Results

5.1 Stability Analysis

To verify the effectiveness of the numerical solution strategy proposed in Section 4, a stability analysis is conducted to compare the numerical results with and without the stabilization method.

The initial state of the crank-slider system positions the crank arm parallel to the ground, while the slider is oriented horizontally at its maximum extension. The parameters for the generalized coordinates at $t = 0s$ and the expected rotational speed are presented in Table 2.

Table 2. Initial condition

x_1	y_1	θ_1	x_2	y_2	θ_2	x_3	ω
30 mm	0 mm	0	150 mm	0 mm	0	240 mm	200rpm

When using direct integration, the graph below shows the variation of generalized coordinates with time from $t = 0$ s to $t = 0.15$ s.

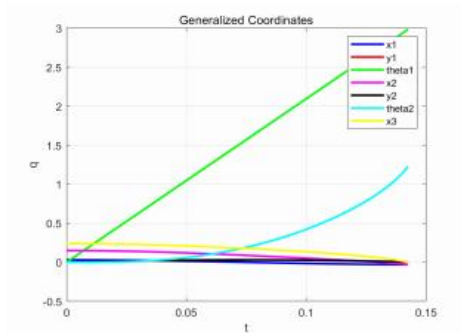


Figure 4. Generalized Coordinates without Stabilization.

The figure demonstrates behavior inconsistent with the expected kinematic response of the system. For example, coordinate θ_2 should decrease over time rather than increase as plotted, while the x coordinate of the slider is shown to reach the origin, a position that is geometrically impossible.

In order to quantify this numerical drift, we define the constraint violation as the modulus of the vector ϕ .

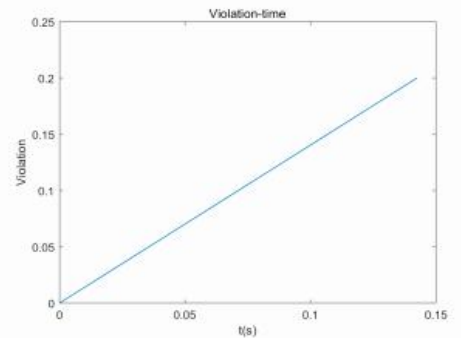


Figure 5. Constraint Violation without Stabilization.

As shown in Figure 5, the violation of the system is increasing monotonically with respect to time, indicating the accumulation of numerical error.

To further investigate the accuracy of the acquired results, we select the generalized coordinate x_3 and compare x_3 's analytical solution with its numerical counterpart, as displayed in Figure 6. The relative error of the two solutions is also computed, and the result is plotted in Figure 7.

In Figure 6, while the analytical solution of x_3 converges at around $t = 0.15$ s, the numerical solution is diverging with decreasing gradient. Figure 7 further demonstrates the phenomenon, showing the rapidly increasing relative error between the two solutions after about $t = 0.1$ s.

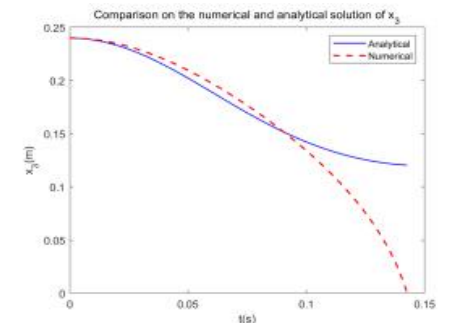


Figure 6. Comparison of the numerical and analytical solutions of x_3 without stabilization.

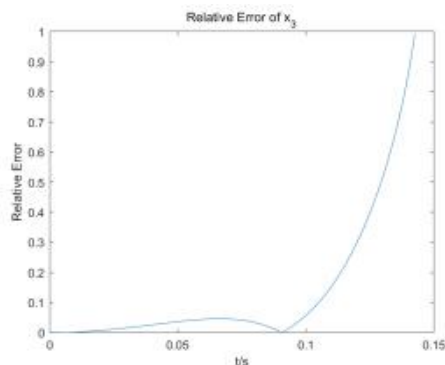


Figure 7. Relative error without stabilization.

In general, the direct integration method fails to provide stable and accurate solutions for the current slider-crank system, highlighting the need to introduce a stabilization method. After using the Baumgarte stabilization method (parameters are set as $\alpha = \beta = 1/\Delta t$ according to experience; their effect on stabilization will be discussed in the next section), the violation of the system is restricted under the value of 1.6×10^{-6} and does not exhibit a diverging trend.

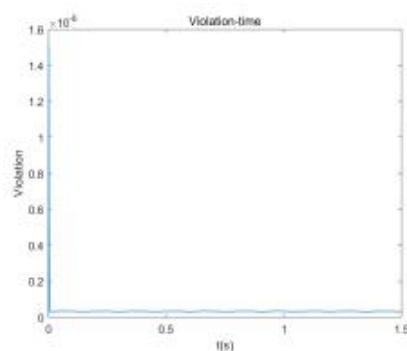


Figure 8. Constraint violation with stabilization.

As for the performance of x_3 , the analytical and numerical solution is found to fit well, exhibiting a relative error under the value of 6×10^{-6} as plotted in Figures 9 and 10. To sum up, the above analysis quantitatively demonstrates that the numerical solution stabilized by the Baumgarte method possesses sufficient accuracy for subsequent dynamic analysis.

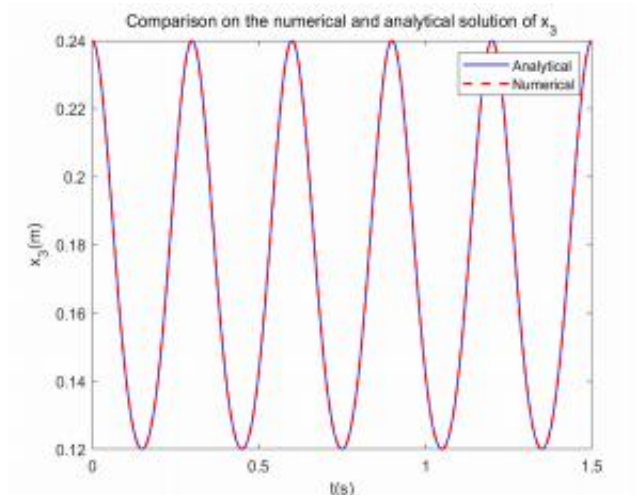


Figure 9. Comparison of the numerical and analytical solution of x_3 after stabilization.

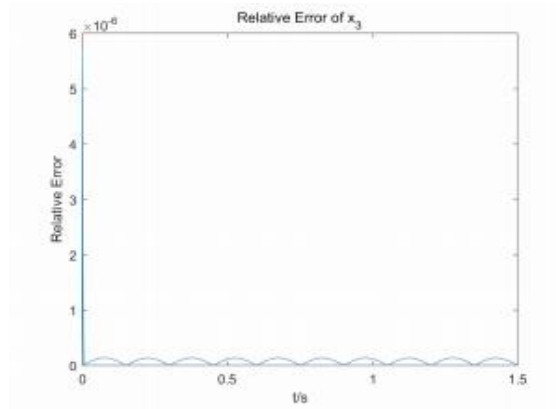


Figure 10. Relative error of x_3 after stabilization.

5.2 Selection of Stabilization Parameters

In the previous sections, all simulations are based on the parameter selection of $\alpha = \beta = 2000$, as the time step Δt is chosen as 0.0005s. We now perform a parameter sweep to find the optimal selection of stabilization parameters.

We shall begin by determining the suitable range for the parameters α and β . It is found that above the value of 2000, there is a rapid divergence of the constraint violation, leading to the destabilization of the system. We therefore set the test α and β to range from 200 to 2000.

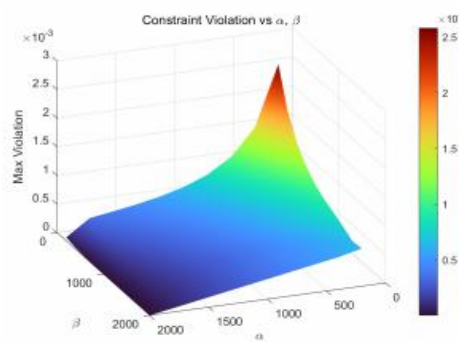


Figure 11. Variation of constraint violation with stabilization parameters.

A simulation is performed that computes the maximum violation obtained during one cycle of rotation under different parameters. The result is plotted above in Figure 11. As shown, increasing the parameters leads to a decrease in constraint violation of the system, and α has a more significant impact. A further figure is plotted to show the effect of β on violation when $\alpha = 2000$ to specify the exact optimal selection. The figure below demonstrates that violation achieves a minimum when $\beta = 2000$.

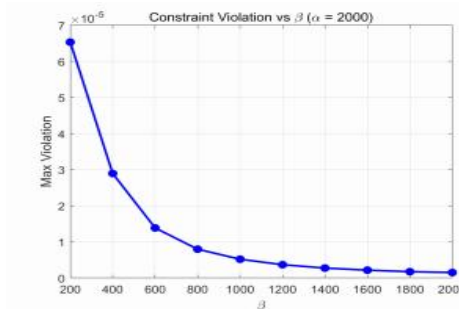


Figure 12. Variation of constraint violation with β when $\alpha = 2000$.

In conclusion, $\alpha = \beta = 2000$ is indeed the optimal solution that leads to minimum constraint violation, while maintaining the stability of the system. We shall select these as the parameters used for the dynamical results.

5.3 Dynamical Results

After introducing the stabilization method and choosing the proper stabilization parameters, we finally investigate the dynamical response of the slider-crank system.

Figure 13 illustrates the variation of 6 generalized coordinates with time (θ_1 is excluded as it will only show a linear increment).

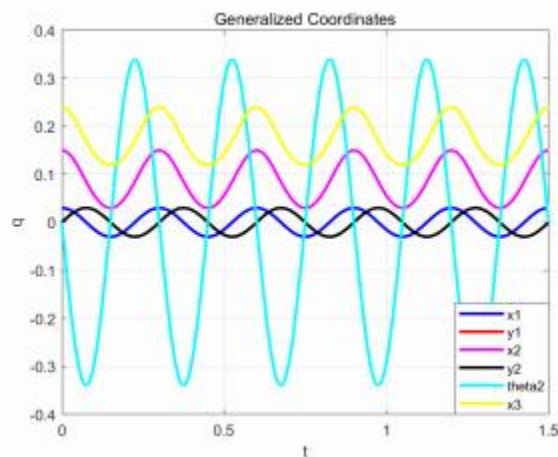


Figure 13. Generalized coordinates after stabilization.

As shown above, the coordinates exhibit smooth periodic oscillations. The period of oscillation is about 0.3s, highly consistent with the theoretical value $T_{theory} = 2\pi(\text{rad})/200(\text{rpm}) = 0.3\text{s}$, calculated based on the expected rotational speed.

The required torque input into the system for constant rotation is also studied. Note that the introduction of α and β in the Baumgarte stabilization method also leads to numerical error in the torque. Hereafter, to study the relationship between the external torque and the generalized coordinate x_1 under different rotational speeds, α and β are fixed to 1000, and the results are plotted in Figure 14.

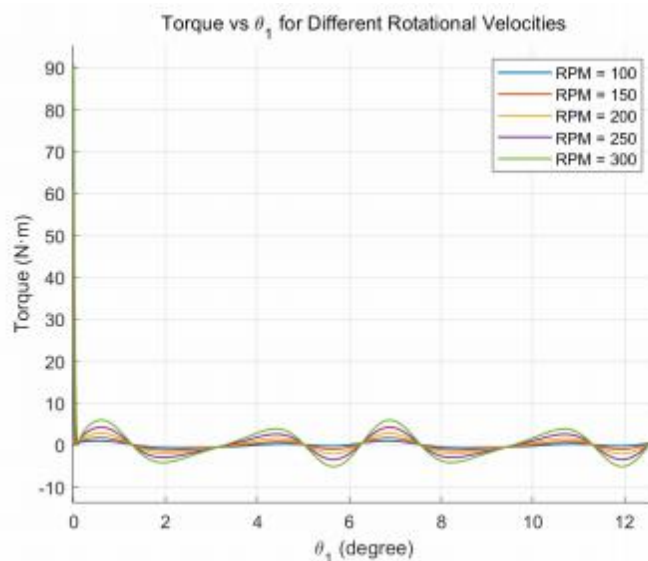


Figure 14. Drive torque.

During the initial phase of simulation ($t < 0.1s$), the drive torque exhibits a transient spike with a significantly high amplitude, approximately 91Nm at 300rpm and 31 at 100rpm. The peak value far exceeds the periodic torque observed after the system reaches steady state. It is because the Baumgarte stabilization method magnifies the initial constraint violation by introducing α and β at a numerical level of 10^3 . Subsequently, the torque rapidly decays and converges to stable periodic oscillations as a function of the crank angle θ_1 . The numerical result shows that one complete cycle occurs over an angular displacement of 6.28 degrees, aligning well with the expected one rotation of 2π . Furthermore, the amplitude of each oscillation, namely the maximum torque required, increases with the rise of rotational velocity, with the exact result displayed below.

Table 3. Maximum torque under different rotational velocities

100rpm	150rpm	200rpm	250rpm	300rpm
1.0232 N·m	1.7969 N·m	2.8819 N·m	4.2790 N·m	5.9892 N·m

6. Conclusion

In conclusion, this paper established a dynamical model on a crank-slider system and developed an efficient numerical solution strategy. We first defined the system's general coordinates, derived the kinematic constraints, and subsequently formulated the equations of motion for the crank-slider system. Order reduction is applied for direct integration, while the Baumgarte Stabilization method is introduced to restrain the numerical drift, and Heun's method is used for integration. A closed loop is formed that repeatedly computes the new generalized coordinates and external torque at the next time step, using the current constraint violation as feedback.

Stability analysis confirmed that constraint violation is controlled at an acceptable numerical level of 10^{-6} after using the Baumgarte method, and a parameter sweep suggested that the optimal stabilization parameter choice is $\alpha = \beta = 2000$. Furthermore, the resulting generalized coordinates exhibit smooth oscillation with a period that aligns well with the theoretical value. The acquired external torque displays stable periodic oscillation after a transient peak arising from the stabilization method, and its maximum value increases with the rise of rotational speed.

The work presents a complete procedure for modeling, simulation, and stability control of a crank-slider system. It verifies the effectiveness of the Baumgarte stabilization method in controlling constraint violation and provides a reliable method for future numerical analysis on similar multi-body systems.

References

- [1] Flores P, Ambrósio J, Claro JCP, Lankarani HM. Kinematics and Dynamics of Multibody Systems with Imperfect Joints: Models and Case Studies. Vol 34. Springer Science & Business Media; 2008.
- [2] Shabana AA. Dynamics of Multibody Systems. Cambridge University Press; 2020.
- [3] Gu P. Chaotic vibration in machine systems and its implications for design [Ph.D. thesis]. Massachusetts Institute of Technology; 1994.
- [4] Wu H, Wu P, Li F, Shi H, Xu K. Fatigue analysis of the gearbox housing in high-speed trains under wheel polygonization using a multibody dynamics algorithm. Engineering Failure Analysis 2019;100:351-64.
- [5] Kane TR, Likins PW, Levinson DA, et al. Spacecraft Dynamics. 1983.
- [6] Dubowsky S, Freudenstein F. Dynamic analysis of mechanical systems with clearances—Part 1: Formation of dynamic model. 1971.
- [7] Khulief YA, Shabana AA. Dynamic analysis of constrained system of rigid and flexible bodies with intermittent motion. Journal of Mechanisms, Transmissions, and Automation in Design 1986;108(1):38-45.
- [8] Shabana A. An absolute nodal coordinate formulation for the large rotation and deformation analysis of flexible bodies. 1996.
- [9] Ye Y, Huang P, Sun Y, Shi D. MBSNet: A deep learning model for multibody dynamics simulation and its application to a vehicle-track system. Mechanical Systems and Signal Processing 2021;157:107716.
- [10] Koutsoupakis J, Seventekidis P, Giagopoulos D. Machine learning based condition monitoring for gear transmission systems using data generated by optimal multibody dynamics models. Mechanical Systems and Signal Processing 2023;190:110130.
- [11] Nikravesh PE. Computer-Aided Analysis of Mechanical Systems. Prentice-Hall, Inc.; 1988.